Applied Geochemistry, Vol. 8, pp. 37–49, 1993
Printed in Great Britain

Pergamon Press Ltd

Implications of rock mineralogy and texture on the feasibility of *in situ* leach mining of Mn-bearing iron formations of central Minnesota, U.S.A.

B. SAINI-EIDUKAT
Institute of Geological Sciences, Mining University, Leoben, A-8600 Leoben, Austria

and

D. MAROZA, R. BLAKE and N. ADAMSON
Geologist, Twin Cities Research Center, Bureau of Mines, Minneapolis, Minnesota, U.S.A.

(*Received* 14 *November* 1991; *accepted in revised form* 20 *May* 1992)

Abstract—The U.S. Bureau of Mines is investigating the feasibility of extracting Mn using *in situ* leach mining methods. Among the deposits being examined are the iron formations of the Cuyuna Range, Minnesota, which contain high-tonnage, low grade deposits of manganese oxides. Manganese minerals identified include pyrolusite, cryptomelane–hollandite, manganite, braunite and lithiophorite. Ore reactivities, as measured by batch leaching tests using aqueous SO_2, are compared to theoretical estimates of the leaching behavior of individual manganese minerals based on kinetic and thermodynamic evaluations. Experimental results in some cases show opposite trends to those predicted by theoretical estimates. In batch leaching tests of Cuyuna Range ores, texture was shown to be of greater importance than thermodynamic reactivity in determining amenability to leaching. Predicting the practical potential for recovery of Mn by *in situ* leaching must involve identification of the effects of texture (massive, fracture-hosted, or interstitial) in addition to ore mineral reactivity.

INTRODUCTION

THE BUREAU of Mines is conducting research on new mining technologies which have the potential of reducing the current high U.S. import reliance on "critical and strategic" elements. These elements (such as Mn, Co, Ni, Al, Cr, and the platinum group), which are essential to domestic industries, occur in low grade or small tonnage deposits in the U.S.A. Conventional mining of these types of deposits may not be possible due to their sensitive environmental location, or due to their low grade, small tonnage, or great depth.

For millennia, extracting metals from the Earth has involved bulk mining and comminution of ore with attendant waste, health, and safety risks. New mining methods that minimize worker exposure to hazardous underground conditions, reduce environmental impacts, reduce waste rock, and allow the economic extraction of low grade or small tonnage deposits of strategic metals are undergoing active research at the Bureau.

One of these methods, *in situ* leach mining, involves circulating dilute chemical solutions through an ore body to selectively dissolve target metals, after which the solutions are pumped to the surface for metal recovery. The comprehensive research program of the Bureau includes: (1) laboratory tests to evaluate deposits for leachability; (2) optimization of the chemistry of leach solutions; (3) evaluation of the potential effects of geology and specifically of lithology and structure to leaching; (4) application of geochemical modeling to solution-rock interactions; (5) hydrological modeling to estimate fluid flow during leaching; (6) development of geophysical techniques to monitor leach solutions; (7) recovery of metals from leach solutions; and (8) post-mining restoration. Inherent in all of these efforts is the consideration of potential environmental impacts of *in situ* leach mining and requirements of regulatory agencies. The principal environmental concern of *in situ* leach mining is in control and collection of the leach solution. Solution control technology is a major part of the research effort.

Understanding both the specific geology of an area (on a scale from regional structure down to mineral texture) and the geochemical reactions which occur between leach solution and host rock minerals is the first step in assessing the potential of an area for *in situ* leach mining. The discussion below highlights this interrelation for leaching Mn: after a discussion of the regional geology of the Cuyuna Range in central Minnesota, data on Mn distribution, mineralogy and texture will be used to interpret leaching tests of Mn-bearing iron formation.

RESEARCH SITE AND PROCEDURE

The iron formations of the Cuyuna Iron Range are typically divided into three districts: the Emily District, the North Range, and the South Range, and

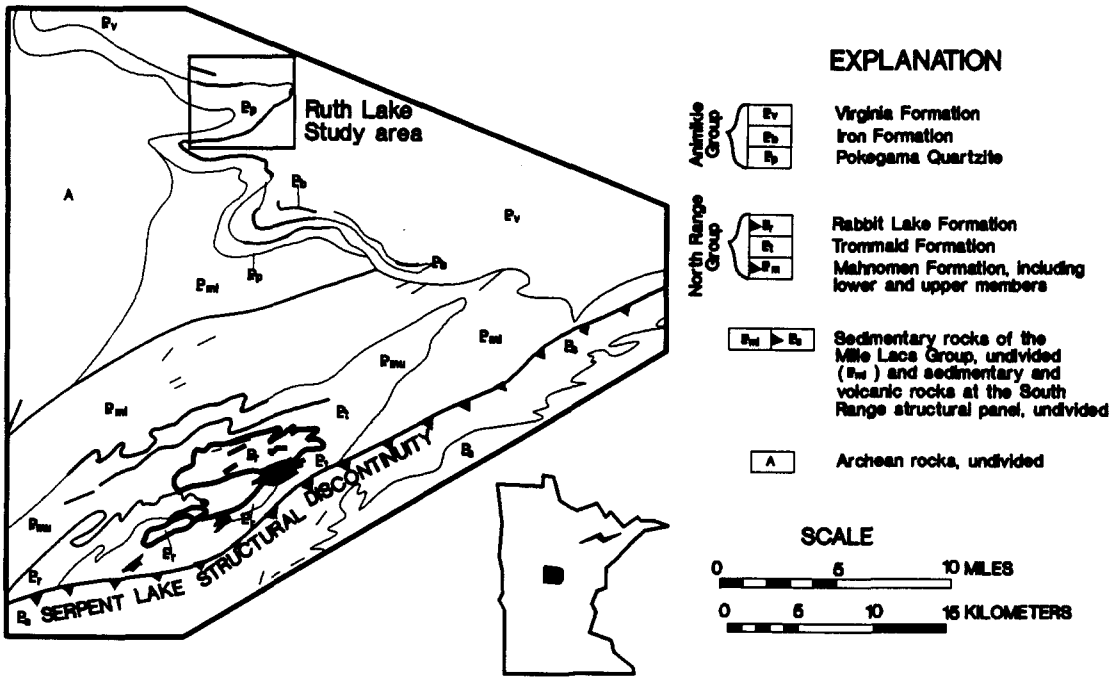

FIG. 1. Location and generalized geological map of the Cuyuna Range and Emily District, after MOREY *et al.* (1991).

contain low grade, high tonnage deposits of manganese oxides (BELTRAME *et al.*, 1981). Although a substantial literature on the bulk dissolution characteristics of manganese ores exists (DAVIS, 1930; ANDERSON, 1942; WYMAN and RAVITZ, 1947; BENDER and RAMPACEK, 1957; DOLEZAL and FULLER, 1959; HENN *et al.*, 1968; RAISONI and DIXIT, 1988; PAHLMAN and KHALAFALLA, 1988), the present study differs from previous work in two key respects. First, most previous research was done from the perspective of leaching Mn from bulk mined ore. The ore was usually crushed and ground, and experimental conditions may not have been comparable to those of *in situ* leaching of bulk rock. Other research, done from a chemical mechanism or chemical kinetic perspective, was usually performed on ground single mineral samples. Second, textural relations between ore and gangue minerals play an important role in ore leaching and must be taken into consideration for proper assessment of potential leachability. This has been documented in detail by Bureau research of *in situ* leaching of copper oxide ores (EARLEY *et al.*, 1990; LARSON *et al.*, 1988; PAULSON and KUHLMAN, 1989 and references therein). The authors are aware of no previous study which has investigated the interaction of leach solution with manganiferous rock from a geological perspective. The current study uses techniques such as reflected light optical microscopy, scanning electron microscopy and electron microprobe analysis to document the compositional and textural changes caused by leach solution–rock interactions. The results provide insight to the relative effects of chemical reactivity and ore texture during the leaching process.

Geology of the Cuyuna Range

The bedrock geology of the Early Proterozoic Cuyuna Range has been discussed most recently by MOREY *et al.* (1991) and SOUTHWICK *et al.* (1988). In general, the iron formation of the Emily District has been correlated with the Biwabik Iron Formation of the Mesabi Range to the northeast (MARSDEN, 1972; MOREY, 1978), and is part of the Animikie Group of quartzite, iron formation, turbidite and graywacke accumulations (Fig. 1). The Animikie Group is interpreted to be the result of deposition in the foreland basin of a Proterozoic collision event, the Penokean orogeny, 1.9–1.76 Ga ago (SOUTHWICK *et al.*, 1988). These rocks unconformably overlie the sedimentary and volcanic rocks of the North Range (SCHMIDT, 1963). Rocks deposited in association with these iron formations vary from shallow-water of sandstone and siltstone in the Emily District to black shale and argillite of the North Range, to volcanic rocks in the South Range (MOREY *et al.*, 1991).

Both the North and South Range and the Emily District iron formations were subjected to natural leaching events which variably oxidized and leached the rocks and concentrated Fe and Mn, while removing Si, Ca, Mg and CO_2. These leaching events may have occurred 1.5–1.6 Ga ago (PETERMAN, 1966) and during Late Jurassic or Early Cretaceous time.

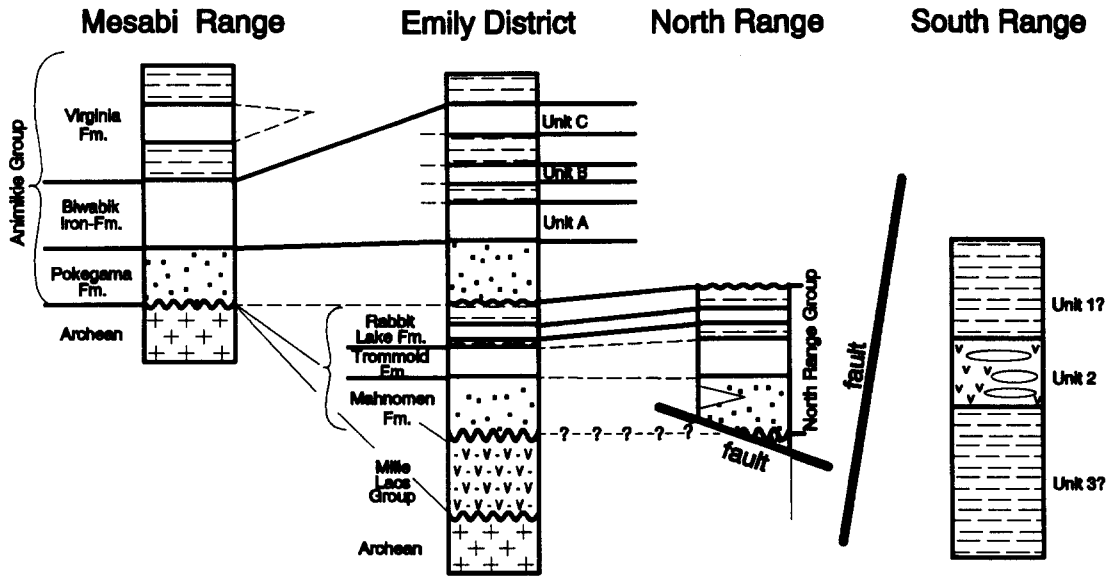

FIG. 2. Stratigraphic column of the Cuyuna Range and Emily District, after MOREY *et al.* (1991).

The North and South Range districts. Structurally, the North Range consists of northeast trending, doubly-plunging synclines with generally steep dips to the southeast. The basal rocks of the North Range group are argillite, siltstone, sandstone and limestone of the Mahnomen Formation (Figs 1 and 2), conformably overlain by the 15–150 m thick Fe-rich and Mn-bearing Trommald Formation (SCHMIDT, 1963). The top of the North Range Group consists of argillite, slate, iron formation and ferruginous slate of the Rabbit Lake Formation.

The Trommald Formation can be divided into two mappable facies, the thick bedded (or granular or cherty), and the thin bedded (or nongranular or slaty). These terms are almost wholly structural (GROUT and WOLFF, 1955) and MOREY *et al.* (1991) give the following explanation:

> The thick-bedded facies is typified by wavy-bedded granule-chert layers ranging in thickness from several centimeters to 2 meters, which are intercalated with thinner beds of hematite or magnetite. The cherty layers consist of ovoid granules of cherty quartz, carbonates, silicates, hematite and magnetite. Matrix material may or may not be mineralogically similar to the granules, ... but is generally rich in quartz. The thin-bedded facies is characterized by bedding laminae generally less than several millimeters thick. Individual layers in this facies are composed of various proportions of quartz, siderite, magnetite, stilpnomelane, minnesotaite, and chlorite ...

Natural oxidation and leaching of the Trommald Formation strongly affected its physical appearance and chemistry (SCHMIDT, 1963; MARSDEN, 1972). Manganese-bearing carbonates and Fe-silicates were converted to hematite, goethite and manganese oxides. The leaching event depleted the rock in CO_2, Ca, Mg and SiO_2 and enriched it in Fe, Al_2O_3 and H_2O relative to unaltered rock. Leached rock exhibits increased porosity, but less than would be expected from the removal of SiO_2 (SCHMIDT, 1963), possibly indicating replacement of SiO_2 by iron oxide.

The thick and thin bedded facies of the Trommald Formation can be interpreted as, respectively, the oxide and carbonate-silicate iron formation facies of JAMES (1955), and it is at the transition between the two facies where the highest Mn values occur (SCHMIDT, 1963). A secondary structural control on the location of large oxidized manganiferous bodies is evidenced by their location in the axial areas of tight folds, where fracturing provided channelways for migrating solutions.

The Emily District. The iron formation succession in the Emily District has been correlated with the Biwabik Iron Formation of the Mesabi Range. It overlies the Pokegama Quartzite, which itself forms the basal unit of the Animikie Group, and underlies the slate and graywacke of the Virginia Formation (Figs 1–3). The Animikie Group unconformably overlies older folded rocks of the North Range and is not correlative with the North Range Group. The stratigraphic succession in the Emily District is folded into a series of broad, open anticlines and synclines with near-vertical axial planes that plunge generally and gently to the north-northeast. In the Ruth Lake Study Area of the Emily District (Fig. 1) the beds dip 15–40° to the north and may flatten in that direction. The strata are broken by north–northeast and west–northwest trending faults with apparent displacements of the order of several tens of meters. Structurally, the Animikie basin forms a broad, eastward-dipping synclinorium, with variable deformation which increases southward.

The stratigraphic succession in which the Mn-

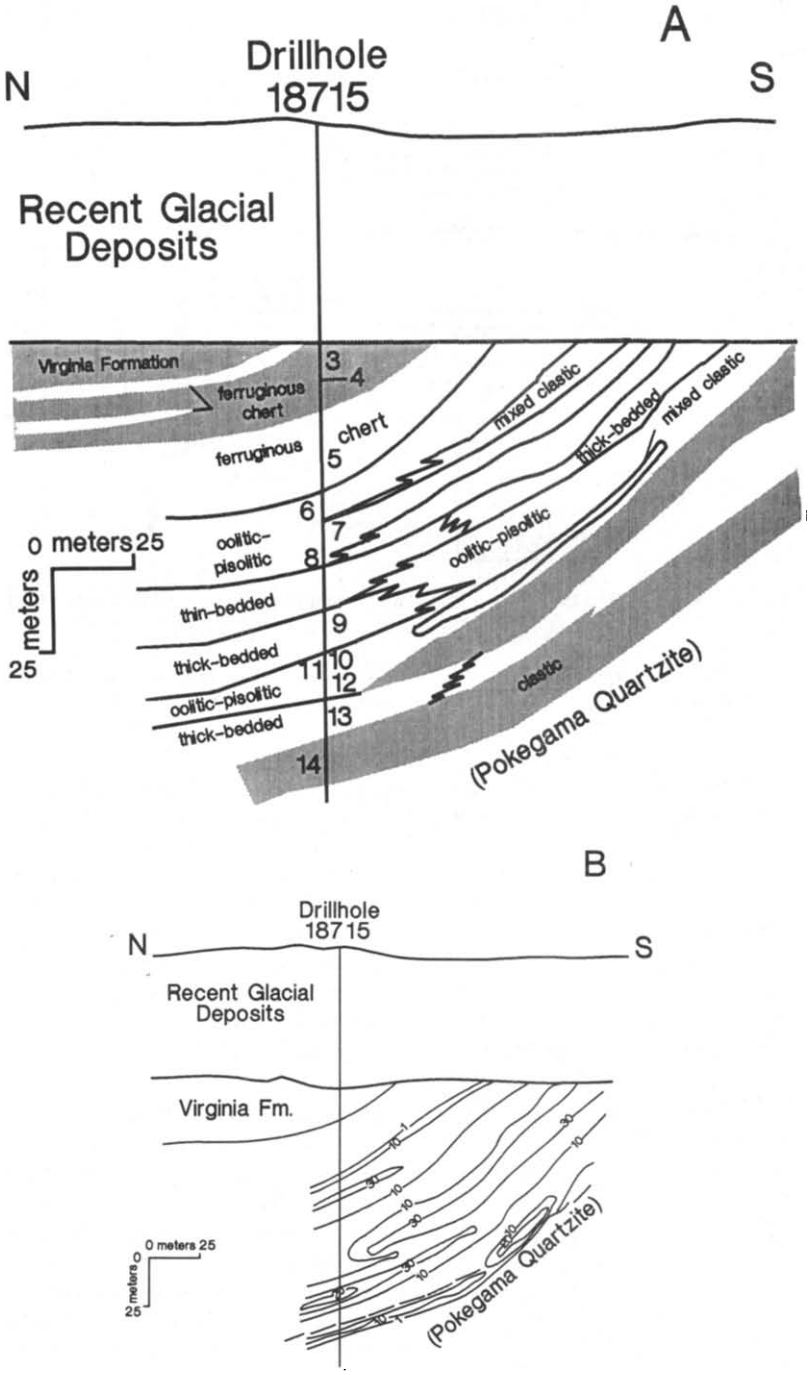

FIG. 3. (A) Generalized cross-sectional distribution of rock types in the Emily District. Numbers correspond to sample numbers in Table 1. Modified from MOREY *et al.* (1991). (B) Generalized cross-sectional distribution of Mn in the Emily District. Numbers label contours of %Mn. Modified from MOREY *et al.* (1991).

bearing rocks of the Emily District occur is discussed in detail by MOREY (1990), and is summarized in Figs 2 and 3. The iron formation in the Emily District can be divided into several rock types, including chert (clastic, algal or jaspery); oolitic or pisolitic; thick-bedded granular; mixed thin-bedded and thick-bedded; and ferruginous chert subunits. The manganese oxides are inferred to have been deposited during early diagenesis by reducing solutions that leached Mn from older rocks in the North Range. The Mn was subsequently reprecipitated in pore spaces in granular parts of the iron formation when the reducing solution encountered oxidizing conditions in the depositional basin. The manganese

oxides were later redistributed by weathering events in late Mesozoic time.

Manganese distribution, mineralogy and texture

Gloria–Zeno Mine (North Range). An example of North Range manganese mineralization is found in an area near the western hinge of the syncline, which includes the Gloria, Zeno and Algoma Mines of SCHMIDT (1963) (Fig. 1). This area was actively mined for iron and manganese ore by both open-pit and underground methods since the late 1800s, but has not seen continuous mining since the late 1970s. Sporadic mining and stockpiling of oxidized manganiferous ore continued throughout the 1980s. Because of the lack of drill core, these ore piles were sampled for mineralogical and geochemical analysis and leaching tests described below.

Drill hole logs on file at the Minnesota Geological Survey indicate that a manganiferous zone continues eastward from the mined area for at least 400 m; however, the stratigraphic relations appear different from that in other areas of the syncline in that most of the manganiferous rock occurs in the thin-bedded facies. SCHMIDT (1963) indicated that the thickness of the thick-bedded facies is unknown in this area and that it may pinch out to the east.

The iron formations and associated rocks of the Gloria–Zeno area have been pervasively leached in some areas. Unoxidized thin-bedded facies rock generally contains 10–15% CO_2, 30–35% SiO_2, 20–30% Fe and 2–5% Mn (MARSDEN, 1972). Plots of SiO_2 vs Mn and Fe using assay data from company drill core logs (Fig. 4) show that in the Gloria–Zeno area, natural leaching has lowered the SiO_2 content of a significant proportion of the rock to <30% and that the highest Mn and Fe contents are associated with the lowest SiO_2 contents. As shown in Fig. 5b, the highest Mn contents are associated with the lowest Fe contents. The triangular-shaped patterns of Figs 4 and 5 are due to the variety of lithologies, from cherty layers to iron or manganese oxide layers to silicate

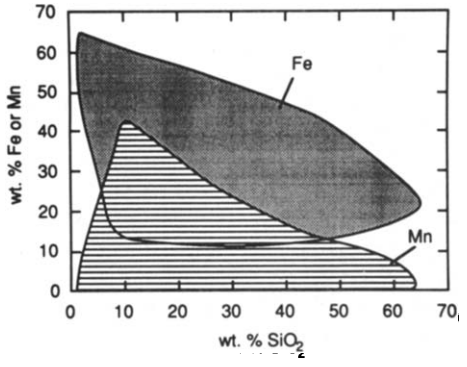

FIG. 4. Variation of Fe and Mn vs SiO_2 in samples from the Gloria–Zeno area. Each area represents 673 data points from mining company drill logs.

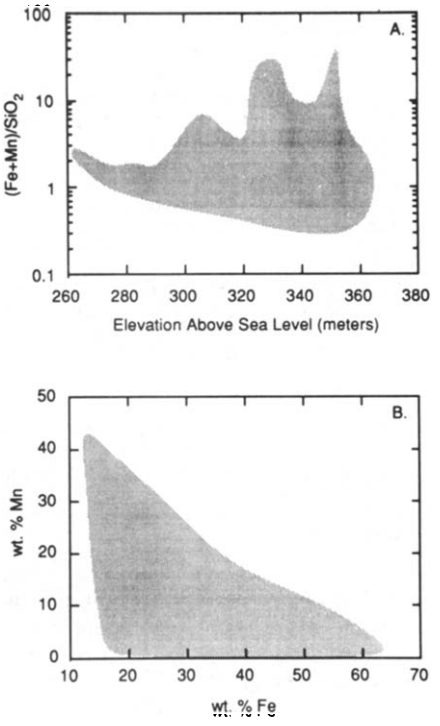

FIG. 5. (A) Distribution of naturally leached iron formation in the Gloria–Zeno area, as shown by variation of [Mn + Fe]/SiO_2 with elevation. (B) Variation of Mn vs Fe in samples from the Gloria–Zeno area. Shaded areas represent 673 data points from mining company drill logs.

layers. Wholerock chemical analyses of Gloria–Zeno Mine stockpile material show very low total C content (Table 1), indicating that leaching has removed almost all original carbonate that may have existed. Where high C contents are found (Table 1, analysis 10), they are due to secondary calcite veins (note that the analytical method used for C cannot distinguish between organic and inorganic C). The extreme variation in (Mn + Fe)/SiO_2 vs elevation (Fig. 5a) indicates that the natural leaching appears to have occurred sporadically throughout the oxidized portion of the deposit, and is not confined to a layer near the surface.

Samples from the Gloria–Zeno Mine stockpiles were divided into two: more manganese-rich and more chert-rich types. The more manganiferous type is thin-bedded with blocky jointing and consists of chert, pyrolusite and hematite in varying proportions. It is highly fractured and contains centimeter-size white quartz segregations. The fibrous to massive and typically radially arranged pyrolusite crystals are usually arranged with their long axes parallel to bedding planes (Fig. 6). Needles of pyrolusite up to 1.5 mm long and only 0.01 mm wide occur in modal abundances which vary considerably from layer to layer. Hematite occurs as subhedral to occasionally euhedral crystals, sometimes in clusters, and range in size from a few microns

Table 1. Whole-rock analyses of Gloria–Zeno and Ruth Lake area samples

Sample	1	2	3	4	5	6	7	8	9	10	11	12	13	14
SiO_2	9.41	67.60	55.62	68.24	8.13	0.45	0.79	21.61	22.89	1.84	6.20	0.64	62.89	76.15
TiO_2	<0.05	<0.05	1.08	1.22	<0.05	<0.05	<0.05	<0.05	<0.05	n.d.	n.d.	<0.05	<0.05	<0.05
Al_2O_3	1.45	0.81	13.42	16.63	0.40	<0.05	0.76	0.38	0.79	0.77	0.59	3.59	2.08	12.66
FeO	<0.13	<0.13	0.90	0.75	0.45	<0.13	<0.13	0.30	<0.13	<0.13	<0.13	<0.13	<0.13	0.45
Fe_2O_3	41.32	28.45	21.16	1.74	80.42	17.87	51.75	67.72	73.49	21.02	0.83	30.60	22.02	2.22
MnO_2	41.62	0.63	<0.05	<0.05	0.49	78.65	42.25	<0.05	0.98	45.57	81.97	58.55	10.13	<0.05
MgO	<0.10	<0.10	0.83	0.99	0.14	<0.10	<0.10	<0.10	<0.10	0.20	<0.10	0.27	<0.10	0.93
CaO	0.45	<0.42	<0.42	<0.42	<0.42	<0.42	<0.42	<0.42	<0.42	10.91	<0.42	1.40	<0.42	<0.42
BaO	n.d.	n.d.	n.d.	n.d.	n.d.	n.d.	0.41	n.d.	n.d.	1.12	0.12	n.d.	n.d.	n.d.
Na_2O	0.23	<0.05	<0.05	<0.05	<0.05	<0.05	0.34	<0.05	<0.05	0.23	0.26	0.40	<0.05	<0.05
K_2O	0.66	<0.05	4.10	5.66	<0.05	<0.05	1.02	<0.05	<0.05	0.90	1.81	2.89	0.16	4.70
P_2O_5	0.05	0.18	0.09	0.08	0.14	0.15	0.13	0.50	0.09	0.20	0.12	0.09	0.19	0.06
S	0.014	<0.005	<0.005	<0.005	<0.005	0.010	<0.005	<0.005	<0.005	<0.005	<0.005	<0.005	0.010	<0.005
C	0.220	0.160	<0.005	<0.005	0.130	0.560	n.d.	n.d.	n.d.	2.600	0.280	<0.005	0.200	<0.005
LOI	3.03	0.83	2.90	3.90	8.60	4.80	2.44	8.40	0.68	16.20	6.80	4.05	3.30	2.10
Total	98.44	98.67	100.09	99.21	98.90	102.48	99.90	98.91	98.92	101.57	98.97	102.47	100.97	99.26

1. Gloria–Zeno stockpile sample (banded texture); 2. Gloria–Zeno cherty stockpile sample; 3–14 Ruth Lake drill core 18715 (see Fig. 3 and Table 3). n.d.—not determined. Analytical method ICP except Fe^{+2} by titrimetric method, SiO_2 gravimetrically, and S, C by LECO combustion method. Analysis of NBS Standard Reference Material 25d (Manganes Ore) gave a value of 81.65 wt% MnO_2 compared to the certified value of 81.94 wt% MnO_2.

to ~30 μ in diameter. Quartz and pyrolusite veins as much as 300 μ wide are oriented perpendicular to the bedding planes. The more chert-rich type of the Gloria–Zeno sample consists of millimeter-thick bedded chert and hematite usually arranged with their long axes aligned at an angle to bedding. Hematite crystals range in size from microns to hundreds of microns in diameter, and the texture of the pyrolusite is generally massive.

Pyrolusite from the Gloria–Zeno Mine samples analyzed by electron microprobe contains >1 wt% each of Fe_2O_3, BaO, CaO and K_2O (Table 2). Lead was the only trace metal analyzed, but with one exception was not found in pyrolusite at levels greater than the detection limit of 0.1 wt%.

Ruth Lake Area (Emily District). Geological estimation of core and churn drilling results in the Emily District has defined a large Mn resource of ~1.7 Mt grading ~10% Mn (Morey *et al.*, 1991). Although much of the iron formation contains at least 1 wt% Mn, two stratigraphic levels contain concentrations of Mn with grades of as much as 50 wt% (Fig. 3). These levels generally conform to the oolitic–pisolitic rock type of Morey *et al.* (1991). The lower zone, which consists of as much as 15 m of mostly cryptomelane, can be traced along strike in drill core for ~1800 m. The upper zone, a lens ~650 m long and as much as 6 m thick, consists predominantly of romanechite ($BaMn_9O_{16}(OH)_4$). Pyrolusite and secondary manganite are found in both zones.

The mineral assemblage of the iron formation (quartz–goethite–hematite–manganese oxide) is maintained throughout the succession, including the Mn-rich zones. In the Mn-enriched zones, the quartz content of the rock varies inversely with the Mn content, but total Fe content tends to remain fairly constant from Mn-poor to Mn-rich layers in the iron formation. (Morey *et al.*, 1991).

Samples of each of the major iron formation types of Morey *et al.* (1991) were taken from U.S. Steel drill core at the Minnesota Department of Natural Resources Division of Minerals Drill Core Library in Hibbing, Minnesota. These samples were chemically analyzed and examined by X-ray diffraction, optical microscopy and electron microprobe (Tables 1, 3 and 4). Manganese minerals identified include manganite (γ-MnOOH), cryptomelane ($KMn_8O_{16} \cdot H_2O$), hollandite ($BaMn_8O_{16} \cdot H_2O$) and braunite ($Mn^{2+}Mn_6^{3+}SiO_{12}$). A probable identification of lithiophorite (simplified formula $(Al,Li)OH_2 \cdot MnO_2$; sample 18715–545) was made by electron microprobe based on mineral stoichiometry (Table 4, Fig. 7).

The textures of the manganese minerals examined vary from massive to intergranular. In some cases, several generations of Mn deposition can be distinguished on the basis of cross-cutting vein relations, many of which exhibit consistently different minor element abundances (Table 4, Fig. 8).

Batch and column leaching tests

As discussed below and in Petrie (1991), aqueous SO_2 has been shown to be an efficient solvent for oxidized Mn ores. Batch and column leaching experiments were performed on samples from the Gloria–Zeno Mine (North Range District) and the Ruth Lake (Emily District) Study Area. Column leaching tests were conducted on 1 m long 10-cm-diameter containing 3.5 kg of minus 2.5-plus 1.3 cm samples (Pahlman and Khalafalla, 1988). A 5 wt% solution of aqueous SO_2 was applied to the top of the column at a rate of 1 ml/min and leach solution samples were collected at the bottom of the column for chemical analysis for Fe, Mn, Si, Ca, Na, K and Al by atomic absorption spectrometry or inductively-coupled plasma spectrometry.

In the batch experiments, ~1 cm^3 cubes were

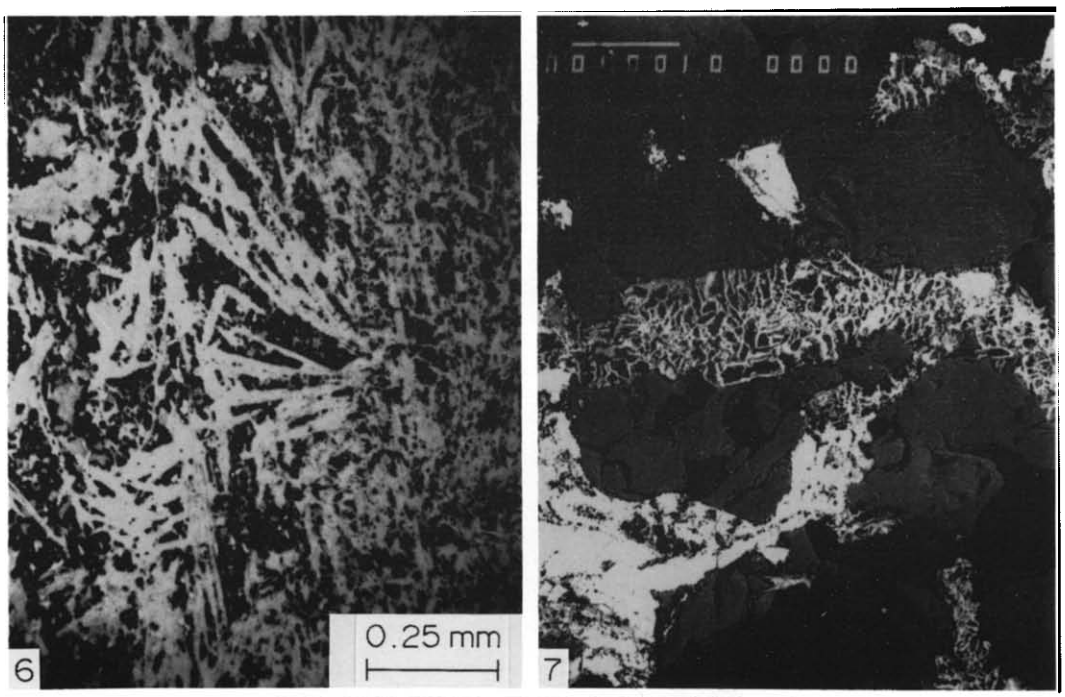

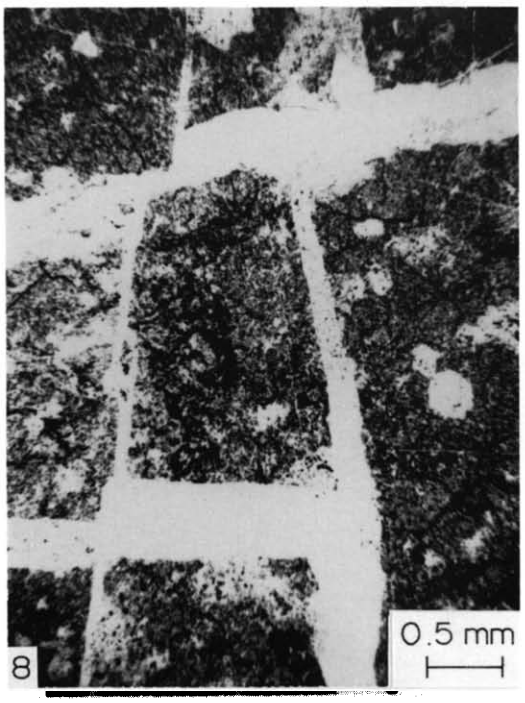

FIG. 6. Photomicrograph of Mn-rich ore from the Gloria–Zeno area. Scale bar is 250 μ. See Tables 1 and 2 for wholerock and mineral analyses.

FIG. 7. Scanning electron micrograph of Emily District sample 18715–545, after exposure to SO_2 solution, showing interstitial texture of the ore. Backscattered electron imaging. Gray-quartz; bright-lithiophorite; net textured material-cryptomelane intergrown with hematite. Scale bar is 100 μ. See Tables 1 and 4 for wholerock and mineral analyses.

FIG. 8. Photomicrograph of sample 18715–373 from the Emily District, showing late cryptomelane veins cutting groundmass of cryptomelane and hematite. Scale bar is 0.5 mm. See Tables 1 and 4 for wholerock and mineral analyses.

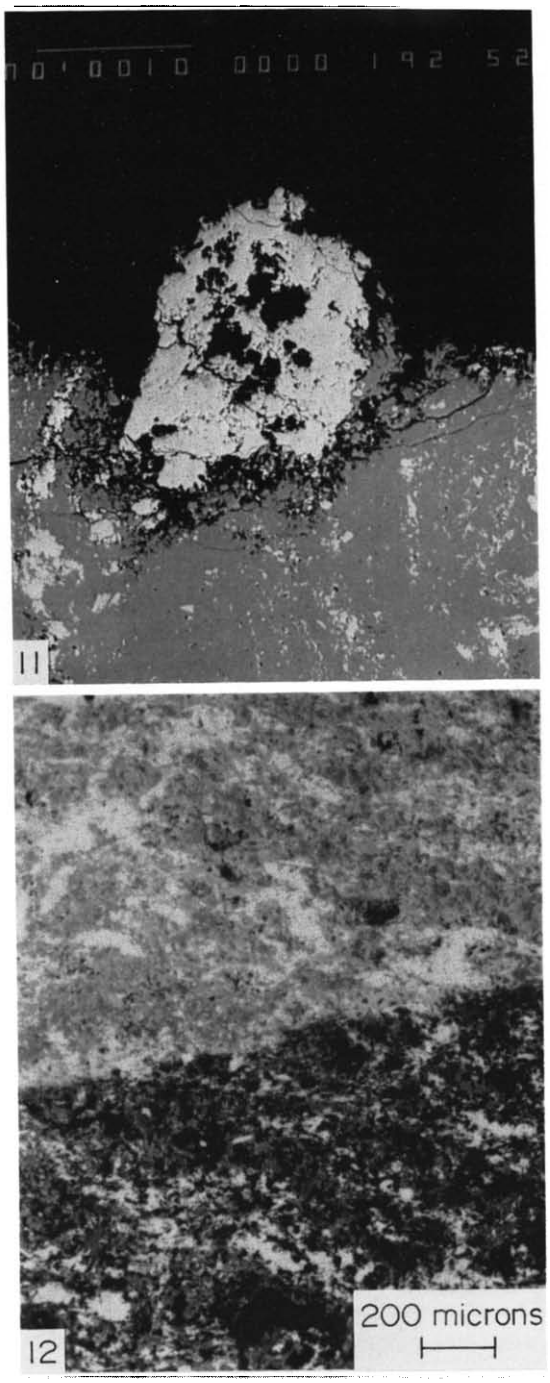

FIG. 11. Scanning electron micrograph of sample 18715–365 after exposure to SO_2 solution. Backscattered electron imaging. Dark—manganite; bright—hematite. Scale bar is 100 μ.

FIG. 12. Scanning electron micrograph of Gloria–Zeno area ore showing textural relations between hematite (bright), quartz (medium dark gray), and pyrolusite after exposure to SO_2 solution. The upper half of the figure shows the unleached ore. Backscattered electron imaging. Scale bar is 200 μ.

Table 2. Representative electron microprobe analyses of pyrolusite from Gloria–Zeno stockpile samples

Sample	1	2	3	4	5	6	7
Wt%							
SiO_2	0.28	0.24	0.19	0.24	0.21	0.30	0.11
Al_2O_3	1.11	1.40	1.28	1.27	0.98	2.72	1.72
Fe_2O_3	1.43	39.59	0.97	1.42	1.09	2.29	1.17
MnO_2	92.25	56.18	92.56	91.89	92.71	88.92	89.82
BaO	0.98	0.66	1.07	1.40	1.25	1.35	2.17
PbO	<0.10	n.d.	<0.10	0.12	<0.10	<0.10	<0.10
CaO	1.61	0.99	1.44	1.32	1.43	1.34	1.16
Na_2O	0.70	0.39	0.67	0.67	0.70	0.59	0.71
K_2O	2.10	1.53	2.36	2.55	2.47	2.37	2.71
Sum	100.46	100.98	100.54	100.88	100.84	99.88	99.57
Atoms							
Si	0.004	0.004	0.003	0.003	0.003	0.004	0.002
Al	0.019	0.026	0.022	0.022	0.017	0.048	0.030
Fe	0.016	0.466	0.011	0.016	0.012	0.026	0.013
Mn	0.939	0.607	0.942	0.937	0.944	0.911	0.932
Ba	0.006	0.004	0.006	0.008	0.007	0.008	0.013
Ca	0.025	0.017	0.023	0.021	0.023	0.021	0.019
Na	0.020	0.012	0.019	0.019	0.020	0.017	0.021
K	0.039	0.031	0.044	0.048	0.046	0.045	0.052

Calculated to two oxygens. Analyses performed on a JEOL Superprobe at 25kV, 15nA using Tracor-Northern phi-rho-z correction methods.

Table 3. Characterization of selected samples from Ruth Lake area

Sample No.	Depth (m)	lithotope* or Fm.	Mn (wt%)	Comments
3	64.6	Virginia Fm	<0.10	Silty graywacke with variable hematite concentration; 25–30% subangular quartz and K-feldspar (50–150 μm diam.); 30–75% clay matrix—mode inverse to hematite mode; 10–35% hematite (10–30 μm) with occasional magnetite cores
4	66.4	Virginia Fm	<0.10	Graywacke: 70% clay matrix, 30% quartz and feldspar grains (15–50 μm diam.) (qtz:feldspar = 4:1). Trace to 1% hematite as μm-size interstitial grains
5	97.5	Ferruginous chert	0.31	95–98% hematite—μm-size crystals to massive texture. 2–5% quartz or voids; trace chalcopyrite; mm-wide fractures cut the sample. No manganiferous phases found by SEM
6	111.3	Oolitic–pisolitic	49.70	Massive manganite replacement containing hematite inclusions. Accessory quartz and barite. Prominent veins crosscutting sample
7	113.7	Oolitic–pisolitic	26.70	Massive cryptomelane, with groundmass of cryptomelane and inclusions of massive to μm sized hematite
8	126.5	Thin-bedded and thick-bedded	<0.10	Quartz, goethite, hematite (cored by goethite and magnetite)
9	140.8	Thick-bedded	0.62	Remnant oolites (250–500 μm diam) of hematite and chert. Microprobe analyses indicate presence of cryptomelane
10	150.0	Oolitic-pisolitic	28.80	Hollandite (80%) with μm-sized inclusions of hematite and goethite, brecciated by veins of calcite
11	150.3	Oolitic–pisolitic	51.80	Groundmass (70%) of braunite I which includes patches of hematite and goethite, and cryptomelane (30%) in relict oolitic textures. Later cross-cutting veinlets of cryptomelane
12	153.9	Oolitic–pisolitic	37.00	Cryptomelane with hematite; porous and leached texture
13	166.1	Thick-bedded	6.40	Granular iron formation. Rounded quartz grains and similarly shaped replacement lithiophorite (100–500 μm diam) with interstitial hematite and cryptomelane

DDH#18715 sampled at the Minnesota Dept of Natural Resources Drill Core Library, Hibbing, MN.
*According to the nomenclature of Morey (1990).

Table 4. Electron microprobe analyses of manganese oxides from the Ruth Lake area

Analysis	1	2	3	4	5	6	7	8	9	10
Mineral sample	Manganite 6	Manganite 6	Manganite 6	Braunite I 6	Crypt 7	Crypt 7	Crypt 9	Hollandite 10	Crypt 12	Lithiophorite 13
wt%										
SiO_2	0.15	0.34	0.36	10.70	0.20	0.19	0.33	0.32	0.60	0.14
Al_2O_3	0.26	1.30	1.15	0.17	0.67	0.61	4.42	0.15	4.17	23.78
Fe_2O_3	0.10	0.15	0.13	6.17	0.12	0.15	1.42	0.44	5.33	0.48
Mn_2O_3	94.45	89.16	97.00	81.73	95.49	96.11	88.42	83.45	83.72	61.42
BaO	1.72	3.46	0.15	0.05	0.62	1.15	0.86	12.88	0.36	0.16
PbO	<0.10	<0.10	<0.10	<0.10	<0.10	<0.10	<0.10	n.a.	n.a.	<0.10
CaO	0.15	0.26	<0.05	1.12	0.17	0.21	0.35	0.66	0.26	0.06
Na_2O	0.63	0.52	0.02	0.04	0.96	0.78	0.67	0.19	0.36	0.02
K_2O	3.12	3.18	0.01	0.06	1.61	1.67	1.71	0.09	4.76	0.08
Li_2O (calc)	—	—	—	—	—	—	—	—	—	2.97
Subtotal	—	—	—	—	99.84	100.87	98.18	98.49	99.94	89.11
H_2O (calc)	—	—	—	—	0.71	0.74	0.75	1.81	1.11	11.49
Total	100.58	98.37	98.83	100.04	100.55	101.61	98.93	100.30*	101.05†	100.60
Atoms										
Si	0.001	0.003	0.003	1.041	0.024	0.023	0.040	0.043	0.074	0.070
Al	0.002	0.012	0.010	0.019	0.095	0.086	0.631	0.025	0.603	13.911
Fe	0.001	0.001	0.001	0.452	0.011	0.013	0.128	0.046	0.493	0.180
Mn	0.978	0.962	0.985	6.056	7.897	7.903	7.391	7.904	7.104	21.067
Ba	0.005	0.011	<0.001	0.002	0.029	0.054	0.041	0.692	0.018	0.031
Ca	0.001	0.002	<0.001	0.117	0.022	0.027	0.045	0.097	0.034	0.031
Na	0.009	0.008	<0.001	0.007	0.223	0.179	0.157	0.052	0.087	0.024
K	0.030	0.032	<0.001	0.008	0.246	0.253	0.265	0.016	0.745	0.050
Li	—	—	—	—	—	—	—	—	—	5.962
Total	1.027	1.031	0.999	7.702	8.547	8.539	8.698	8.938‡	9.228§	41.326
No. analyses	6	3	6	19	7	3	3	5	6	18

Notes: crypt: cryptomelane. Samples from drill core 18715 (see Fig. 3A). 1–4: Mn as Mn^{+3}; 5–10: Mn as Mn^{+4}. 1—Manganite vein—outer; 2—Manganite vein—inner; 3—Manganite late crosscutting vein; 4—Braunite I in groundmass; 5—Cryptomelane vein crosscutting groundmass; 6—Cryptomelane grains with relict oolitic texture; 7—Cryptomelane grains; 8—Hollandite groundmass and veinlets; 9—Cryptomelane; 10—Lithiophorite grains.

* includes 0.31 MgO;

† includes 0.38 MgO;

‡ includes 0.063 Mg.

§ includes 0.070 Mg. n.a.—not analyzed. 1–3 calculated on a basis of 3 O; 4 calculated on a basis of 12 O; 5 calculated on a basis of 32 + charges; 10 calculated on a basis of 126 + charges. Method of calculating H_2O and Li: for cryptomelane-hollandite, the number of atoms of OH was set equal to [Na + K + (2 × (Ca + Ba)], which was converted to H_2O and divided into the calculated atomic weight of the mineral to produce wt% H_2O. For lithiophorite, Li was calculated assuming a ratio of 6 Li atoms per 14 Al atoms, based on the formula of PAULING and KAMB (1982): $Al_{14}Li_6(OH)_{42}\cdot Mn_3^{2+}Mn_{18}^{4+}O_{42}$. For H_2O, the number of atoms of OH was set equal to [3 × (Si + Al + Fe + Ba + Ca + Na + K], which was converted to H_2O and divided into the calculated atomic weight of the mineral to produce wt% H_2O.

suspended in 1-l Erlenmeyer flasks containing 5 wt% SO_2 solution. Ten milliliters of leach solution were extracted periodically using a filtered syringe and were replaced with fresh leach solution. The temperature of the leach solution and pH were monitored and stirring rates were constant for all experiments.

RESULTS

Results for a column leach test of Gloria–Zeno pyrolusite ore are presented in Fig. 9. A Mn recovery of ~90% was achieved, and Mn selectivity was excellent, with the resulting leach solution having a Mn/(Mn + Fe) ratio of generally >0.95. Recovery of Si was extremely low, and although percent recovery of Al and Ca were ~20 and 30%, respectively, the absolute concentration in solution was in the 50–250 ppm range.

Both thermodynamic and kinetic analysis (PETRIE, 1991) and single mineral leaching tests (PAHLMAN and KHALAFALLA, 1988) of Mn–SO_2 dissolution reactions predict that cryptomelane and pyrolusite should leach at approximately the same rate and that manganite should leach more slowly than pyrolusite. Batch leaching experiments were conducted on Gloria–Zeno pyrolusite ore and on Emily District manganite

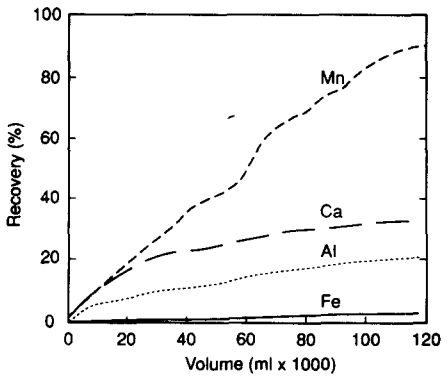

FIG. 9. Percent recovery vs solution volume for Gloria–Zeno column leach test.

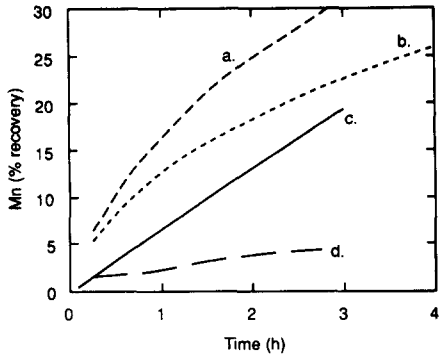

FIG. 10. Percent Mn recovery vs time for Gloria–Zeno and Emily District batch leach tests. (a) cryptomelane, sample 12; (b) pyrolusite, Gloria–Zeno massive texture (30.2 wt% Mn); (c) manganite, sample 6; (d) pyrolusite, Gloria–Zeno banded texture (26.3 wt% Mn).

and cryptomelane ores to test the leaching rates of wholerock samples. Figure 10 is a plot of Mn recovery vs time for the batch leach tests of both Gloria–Zeno and Emily District ore samples. As shown, there is a wide variation in leaching rates and no specific correlation to rates predicted by kinetic analysis or single mineral leaching tests. For example, the Emily District cryptomelane ore leached more quickly than the Gloria–Zeno pyrolusite ores, and the Emily manganite ore leached more quickly than one of the Gloria–Zeno pyrolusite ores and more slowly than the other. When examined microscopically, the pyrolusite occurs in a texture much less conducive to fluid interaction (Fig. 6) than the cryptomelane. The effect of rock textures on overall leachability of manganese oxides may be the explanation of the lack of correlation of wholerock leaching efficiency to predictions made from kinetic analysis of individual mineral reactivity.

Batch leaching tests were also made of Gloria–Zeno stockpile ore with the same mineralogy but different textures (compare curves b and d, Fig. 10). The texture of the manganese oxide in the higher grade sample (30.2 wt% Mn) was massive as opposed to that of the lower grade sample (26.3 wt% Mn) which was arranged in layers typical of North Range iron formation lithologies described above in the section on North Range mineralogy. Recognizing the absence of accurate information on the change of dissolution rates with increasing ore grade, the results (Fig. 10) lead to the conclusion that ore texture is an overriding factor in Mn recovery.

Microscopic examination of ore samples leached in SO_2 highlights the physical processes by which dissolution occurs. In one laboratory leaching test a massive manganite ore which contained hematite inclusions was leached with SO_2. A thin section of the ore after leaching is shown in Fig. 11. Leaching has preferentially dissolved the host manganite leaving the hematite grains unaffected. In pyrolusite–hematite–quartz ore, a similar process was observed leaving a residue of hematite and quartz (Fig. 12). In the case of the batch leaching of cryptomelane ore from the Emily District, the residue of hematite and quartz was left suspended in the flask after all the cryptomelane had been dissolved. Lithiophorite appears unaffected by SO_2 solution (Fig. 7).

DISCUSSION

SO_2 *leaching mechanism*

PETRIE (1991) discussed in detail the results of previous research on the dissolution of manganese minerals and ores by selective dissolution with dissolved SO_2 and offered the following conclusions: (1) manganese oxide leaching reactions must involve the reduction of Mn^{3+} and Mn^{4+} to thermodynamically stable and soluble Mn^{2+}; (2) aqueous SO_2 is an effective reductant and has been shown to rapidly dissolve manganese minerals; and (3) SO_2 preferentially selects manganese oxides for dissolution before oxides of Co, Ni, Fe and other transition metals in ocean nodules and in low-grade manganese oxide ores. During the reductive dissolution of manganese oxides, two separate leaching reactions, which occur simultaneously, have been identified

$$Mn^{4+}O_{2(s)} + S^{4+}O_{2(aq)} = Mn^{2+}_{(aq)} + S^{6+}O^{=}_{4(aq)} \quad (1)$$

$$Mn^{4+}O_{2(s)} + 2S^{4+}O_{2(aq)} = Mn^{2+}_{(aq)} + S^{5+}_{2}O^{=}_{6(aq)}. \quad (2)$$

Reaction 1, which forms sulfate ($SO_4^=$) consumes one mole of S for every mole of Mn dissolved, whereas reaction 2, forms dithionate ($S_2O_6^=$) and consumes two moles of S for every mole of Mn dissolved. The percentages of $SO_4^=$ and $S_2O_6^=$ produced during leaching depend on the structure of the manganese oxide mineral, pH and the oxygen content of the solution (PETRIE, 1991).

Although efficient leaching of manganese oxide minerals requires reduction of Mn^{3+} and Mn^{4+} to soluble Mn^{2+}, pH is also a factor because it controls S speciation. Figure 13 is a speciation diagram of the SO_2–HSO_3^-–$SO_3^=$ system vs pH. Sulfurous acid behaves as a weak diprotic acid in which the variation of the concentration of the species SO_2, HSO_3^- and $SO_3^=$ varies as a function of pH (Fig. 13, left-hand vertical axis). Aqueous SO_2 is the reactive S specie in this system. The vertical axis on the right-hand side of Fig. 13 shows the amount of Mn extracted from cube leach tests when the pH of a 5 wt% SO_2 solution was adjusted to 1, 2, 4.5 and 6. The experiments show that Mn extraction can be related to the S speciation in solution. Sulfur is predominantly in the reactive SO_2 form only when pH is <2.5. At higher pH, SO_2 reacts to form HSO_3^- and $SO_3^=$ as shown in Fig. 13. Because

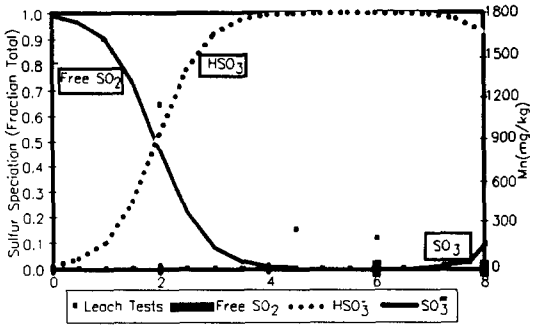

FIG. 13. Speciation of SO_2 with pH (left axis) and experimental dissolution of Mn from Gloria–Zeno ore at differing pH (right axis). Increasing the pH of the leach fluid minimizes SO_2 volatilization because most S is as HSO_3^-; as SO_2 is reacted with ore, more SO_2 is supplied by conversion from HSO_3^-.

higher pH shifts the SO_2 equilibrium toward HSO_3^-, leaching at higher pH also lowers the concentration of SO_2 in solution and slows the bulk dissolution rate. These results indicate that the reductive dissolution of manganese oxides is optimal at low pH.

Dissolution of rhodochrosite ($MnCO_3$), rhodonite ((Mn,Fe,Ca)SiO_3) and most gangue minerals associated with manganese oxide ores does not involve reduction by SO_2 but rather is dependant on the amount of excess acid available for hydrolysis. Gangue dissolution is minimized at high pH. A balance must be achieved between Mn reduction and gangue dissolution to maintain optimum Mn grades in effluent fluids while minimizing contamination by gangue dissolution.

Implications for in situ *leach mining*

The success of evaluating any deposit for its potential as an *in situ* leach mining target depends on the leachability of the metal of interest. This work has shown that the most efficient Mn dissolution occurs when most of the S in solution is as dissolved SO_2 at low pH. However, two negative effects are associated with the conditions of optimal leaching by SO_2: (1) $SO_{2(g)}$ tends to leave solution and enter the atmosphere, resulting in a loss of S from the system. This volatilization effect increases with increasing temperature. For a commercial *in situ* leaching operation, loss of SO_2 due to volatilization could be a financial consideration; (2) the conditions under which optimal manganese oxide mineral leaching occurs coincidentally favor acid dissolution of gangue minerals, even though the Mn dissolution reaction is not an acid-base reaction.

One possible method of optimizing the leaching of manganese oxide with sulfurous oxide is to buffer the pH of the leach solution to as high a value as possible to minimize both effects previously mentioned. At intermediate pH, most of the S could be "stored" as HSO_3^-, and is thus not susceptible to loss by volatilization. The remaining fraction of S would be present as reactive SO_2. In an appropriately buffered system, upon reaction with Mn oxide minerals, reactive SO_2 would be replaced by S converted from HSO_3^-. Also, at intermediate pH less gangue dissolution would occur.

This work has also shown that predicting the leachability of manganese oxide deposits must consider the effects of initial rock texture (massive, fracture-hosted or interstitial) and host rock permeability and porosity, in addition to ore mineral reactivity. Other factors which might change during the leaching process, such as porosity during leaching, must, of course, be considered during the design of an *in situ* leaching program.

Finally, the liberation of mineral inclusions as the manganiferous matrix is dissolved (Fig. 11) may have implications for the flow permeability of the bulk rock under *in situ* conditions. As submicron-sized insoluble mineral grains are freed from their matrix, they may migrate to constricting points in flow paths and reduce effective permeability. This effect may be countered by solutions being forced from flow channels into the rock matrix where it will dissolve matrix manganese minerals and create new flow channels.

Geochemical engineering has been defined (SCHUILING, 1990) as a technology where the natural environment is conditioned by geochemical means to cause a desired result. In the case of *in situ* leach mining, geochemical processes are taken as the starting point from which mining technologies are developed. Thorough knowledge of ore texture, mineralogy, mineral stability, and mineral solubility on a microscopic and a regional scale is essential to engineering successful leach mining programs.

Acknowledgements—The authors acknowledge G. B. Morey and P. W. Weiblen for helpful discussions and criticisms. Constructive comments by reviewers from the Bureau of Mines and from Applied Geochemistry helped to improve the paper. We thank the Minnesota Department of Natural Resources Division of Minerals for providing access to core samples used in this study.

Editorial handling: Brian Hitchon.

REFERENCES

ANDERSON C. T. (1942) Laboratory experiments on sulfur dioxide–sulfuric acid leaching of black and brown manganiferous iron ores of the Cuyuna Range of Minnesota. Manganese Investigations—Metallurgical Division. 14. Hydrometallurgical Studies of Manganese Ores. BuMines RI 3649.

BELTRAME R. J., HOLTZMAN R. C. and WAHL T. E. (1981) Manganese resources of the Cuyuna Range, east-central Minnesota. Minnesota Geol. Surv. Rept of Invest. 24.

BENDER F. N. and RAMPACEK C. (1957) Percolation leaching of manganese ores with sulfur dioxide. BuMines RI 5323.

DAVIS C. W. (1930) Dissolution of various manganese minerals. BuMines RI 3024.

DOLEZAL H. and FULLER H. C. (1959) Acid-ferrous sulfate leaching of low-grade manganese carbonate and oxide ores, Cuyuna Range, Minnesota. BuMines RI 5442.

EARLEY D. E. III, PAULSON S. E. and BRINK S. E. (1990) The effects of rock mineralogy, chemistry, and texture on *in situ* leaching of oxide copper ores from the Santa Cruz Deposit, Arizona. SME/AIME Preprint 90–182.

GROUT F. F. and WOLFF J. F. SR (1955) The geology of the Cuyuna District, Minnesota: a progress report. Minnesota Geol. Surv. Bull. 36.

HENN J. J., KIRBY R. C. and NORMAN L. D. JR (1968) Review of major proposed processes for recovering manganese from United States Resources, Part 3. Sulfur Oxide Processes. BuMines IC 8368.

JAMES H. L. (1955) Sedimentary facies of iron formation. *Econ. Geol.* **49**, 235–293.

LARSON W. C., AHLNESS J. K. and PAULSON S. E. (1988) The Bureau of Mines' role in the development of true *in situ* copper mining as a future technology. *Min. Res. Eng.* **1**, 171–180.

LUTHER G. W. (1990) The frontier molecular orbital theory approach in geochemical processes. In *Aquatic Chemical Kinetics* (ed. W. STUMM), pp. 173–198, Wiley.

MARSDEN R. W. (1972) Cuyuna District. *Geology of Minnesota: a Centennial Volume* (ed. P. K. SIMS and G. B. MOREY), pp. 227–293. Minnesota Geol. Surv.

MOREY G. B. (1978) Lower and middle Precambrian stratigraphic nomenclature for East-Central Minnesota. Minn. Geol. Surv. Rept of Invest. 21.

MOREY G. B. (1990) Geology and manganese resources of the Cuyuna Range, East-Central Minnesota. Minn. Geol. Surv. IC 32.

MOREY G. B., SOUTHWICK D. L. and SCHOTTLER S. P. (1991) Early Proterozoic iron formation and associated manganiferous zones of the Ruth Lake Area, Emily District, Cuyuna Iron Range, East-Central Minnesota. Minn. Geol. Surv. RI 39.

PAHLMAN J. E. and KHALAFALLA S. E. (1988) Leaching of domestic manganese ores with dissolved SO_2. BuMines RI 9150.

PAULING L. and KAMB B. (1982) The crystal structure of lithiophorite. *Am. Miner.* **67**, 817–821.

PAULSON S. E. and KUHLMAN H. L. (1989) Laboratory core leaching and petrologic studies to evaluate oxide copper ores for *in situ* mining. In Bureau of Mines. *In Situ* Leach Mining. BuMines IC 9216, 18–36.

PETERMAN Z. E. (1966) Rb-Sr dating of Middle Precambrian metasedimentary rocks of Minnesota. *Geol. Soc. Am. Bull.* **77**, 1031–1043.

PETRIE L. (1991) Lixivient selection for manganese *in situ* leach mining: a geochemical approach. BuMines Open File Rept 6–91.

RAISONI P. R. and DIXIT S. G. (1988) Leaching of manganese ore with aqueous sulfur dioxide solutions. *Bull. Mater. Sci.* **10**, 479–483.

SCHMIDT R. G. (1963) Geology and ore deposits of the Cuyuna North Range of Minnesota. U.S. Geol. Surv. Prof. Paper 407.

SCHUILING R. D. (1990) Geochemical engineering: some thoughts on a new research field. *Appl. Geochem.* **5**, 251–262.

SOUTHWICK D. L., MOREY G. B. and MCSWIGGEN P. L. (1988) Geologic map of the Penokean Orogen, Central and Eastern Minnesota, and accompanying text. Minn. Geol. Surv. RI 37.

WYMAN W. F. and RAVITZ S. F. (1947) Sulfur dioxide leaching tests on various western manganese ores. BuMines RI 4077.